Inorganic Chemistry

pubs.acs.org/IC Article

Insights on Covalent Attachment of a Re Bipyridyl Catalyst onto *p*-Si(111) Using an Alkyl Linker for Photoelectrochemical CO_2 Reduction

Byunghoon Lee,[‖] Christopher J. Miller,[‖] Jessica G. Freeze, Rajiv Ramanujam Prabhakar, Glenda Chen, Saya Okuno, Julianne S. Lampert, Victor S. Batista, and Clifford P. Kubiak*

Cite This: *Inorg. Chem.* 2026, 65, 9669−9679 Read Online

ACCESS | Metrics & More | Article Recommendations | Supporting Information

ABSTRACT: Re(bpy)$(CO)_3$Cl with a hexyl chain linker was covalently attached to p-type Si(111) via Si−C bond using an organolithium route and confirmed by XPS and ATR-FTIR. Cyclic voltammetry (CV) shows two single-electron reductions with estimated photovoltages of 320 mV and 400 mV for the first and second reductions, respectively. Both reductions were shifted by approximately 200 mV to more positive potentials relative to the homogeneous analogue measured with a methyl-terminated p-type Si(111). CV in a concentrated Cl^- solution indicated that the reformation of the Re−Cl bond is slow, indicating a kinetic barrier in reactivity at the active site. DFT geometry optimizations suggest that under negative bias the complex preferentially adopts configurations that move farther from the methylated Si surface, with the Re−Cl bond oriented parallel to it. Under CO_2, only slight catalytic current enhancement was observed. Controlled-potential electrolysis (CPE) at −2.3 V vs $Fc^{+/0}$ yielded Faradaic efficiencies (FEs) of 15% for CO and 54% for H_2, compared to ∼100% FE for CO observed in the homogeneous system. The selectivity shift is best explained by the dominance of HER at the native Si surface, while CO formation remains limited by slow EC kinetics at the active site of the immobilized Re complex.

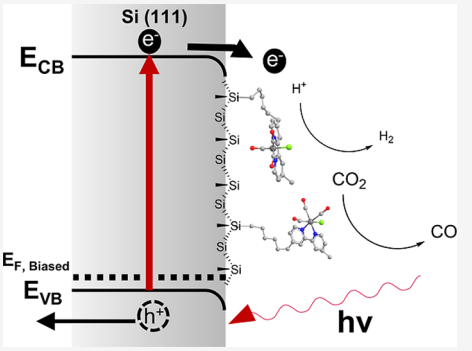

INTRODUCTION

The realization of efficient strategies for harnessing renewable energy from CO_2 reduction will be transformative in achieving carbon neutrality.[1,2] One promising and efficient strategy is to incorporate semiconductors with molecular catalysts to develop a hybrid molecular/semiconductor system in which the light absorbed by the semiconductor can compensate for the large overpotential required for the CO_2 reduction reaction.[3,4]

Previously, our group demonstrated a selective reduction of CO_2 to CO using the Re(bpy-^{t}Bu)$(CO)_3$Cl catalyst and a p-type silicon photocathode.[5] This system achieved approximately 600 mV of photovoltage and reduced the energy input from the applied potential, highlighting the energy efficiency of using a semiconductor photocathode in a homogeneous setup. However, reliance on homogeneous catalysts presents challenges, including issues with catalyst stability and recovery, and limited solvent choices, making the system difficult to scale up for practical use.[6]

There is great interest in transitioning from a homogeneous catalyst platform to the development of robust, selective, and efficient hybrid heterogeneous materials via the immobilization of molecular catalysts onto solid support substrates.[7−9] Ideally, immobilizing molecular catalysts on a surface yields more efficient and effective catalytic materials. The anchoring of the electrocatalyst onto the surface can lead to lower catalyst loading, facilitate heterogeneous electron transfer from the substrate to the catalyst, and enhance selectivity when compared to heterogeneous extended solids, which are known for their range of active sites with varying properties.[10,11] Toward this end, we sought to attach Re(2,2′-bpy)$(CO)_3$Cl type molecular electrocatalyst to a semiconducting surface and investigate its photoelectrochemical CO_2 reduction activity.

Semiconductor properties of doped silicon are well studied and have been used as electrodes in electrochemical and photoelectrochemical cells. Various synthetic processes have been used to modify the surface of Si with functional groups via Si−C bonds, thereby imparting greater passivation against oxidation and enabling extensive studies of Si as a photoelectrode in an electrochemical setup.[12,13] Hydrosilylation,[14−16] organolithium,[17,18] and Grignard chemistry[19,20] are well-established methods for functionalizing organic molecules on Si surfaces. In this study, we employed the Grignard and

Received: March 6, 2026
Revised: April 6, 2026
Accepted: April 9, 2026
Published: April 21, 2026

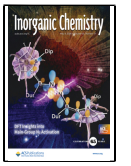

https://doi.org/10.1021/acs.inorgchem.6c01231
Inorg. Chem. 2026, 65, 9669−9679

Scheme 1. Covalent Surface Attachment of Re Bipyridyl Complex on Si(111) Surface Using Organolithium Reaction and Grignard Chemistry

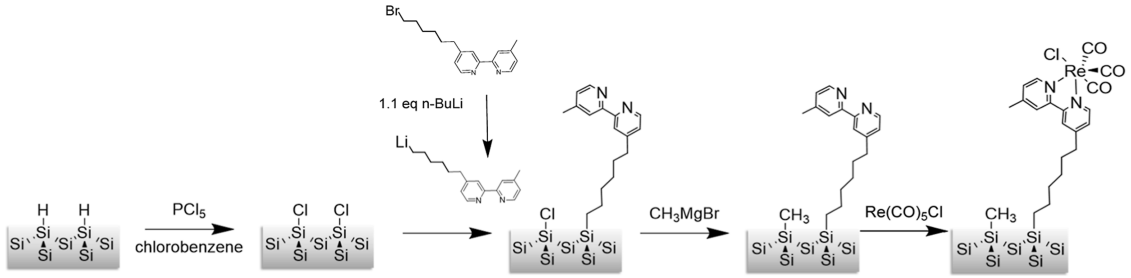

Scheme 2. Synthesis of Bipyridine Ligand with Hexyl Linker. R = H for Ligand for Homogeneous Re(4-Hexyl-4′-methyl-2,2′-bipyridine) Complex. R = Br for Bromine Terminated Version for Attachment

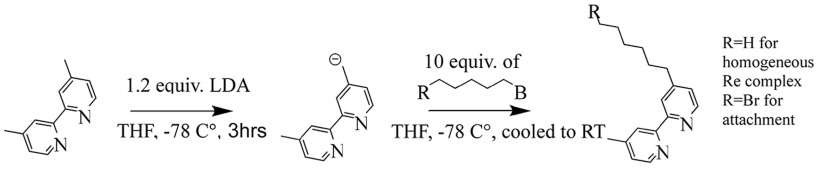

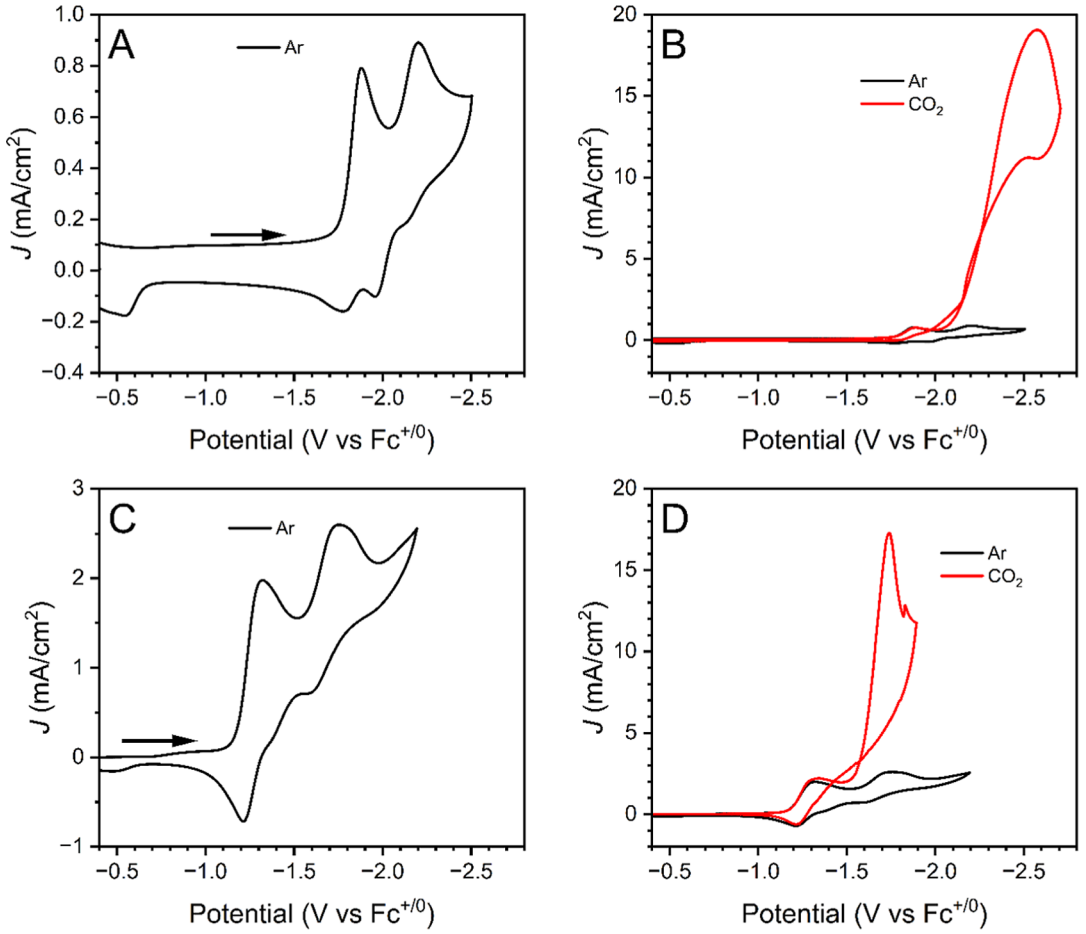

Figure 1. Cyclic voltammogram of Re(bpy-4-hexyl)$(CO)_3Cl$ in dry MeCN with 0.1 M $[Bu_4N][PF_6]$ with glassy carbon WE (A and B) and methylated Si(111) surface as WE (C and D). The Re complex concentration was 2 mM when using a glassy carbon working electrode and 6 mM when using a methylated Si working electrode. Comparison under CO_2 (red) and Ar (black) was shown on the right side. All experiments were conducted with Ag/$AgNO_3$ reference electrode, graphite counter electrode. Ferrocene was used as an internal reference. Scan rate = 100 mV/s. The methylated Si cathode was illuminated with 660 nm laser LED with 15 mW/cm^2 power.

organolithium reaction (Scheme 1) to ensure reliable covalent

attachment of the rhenium catalyst.

https://doi.org/10.1021/acs.inorgchem.6c01231
Inorg. Chem. 2026, 65, 9669−9679

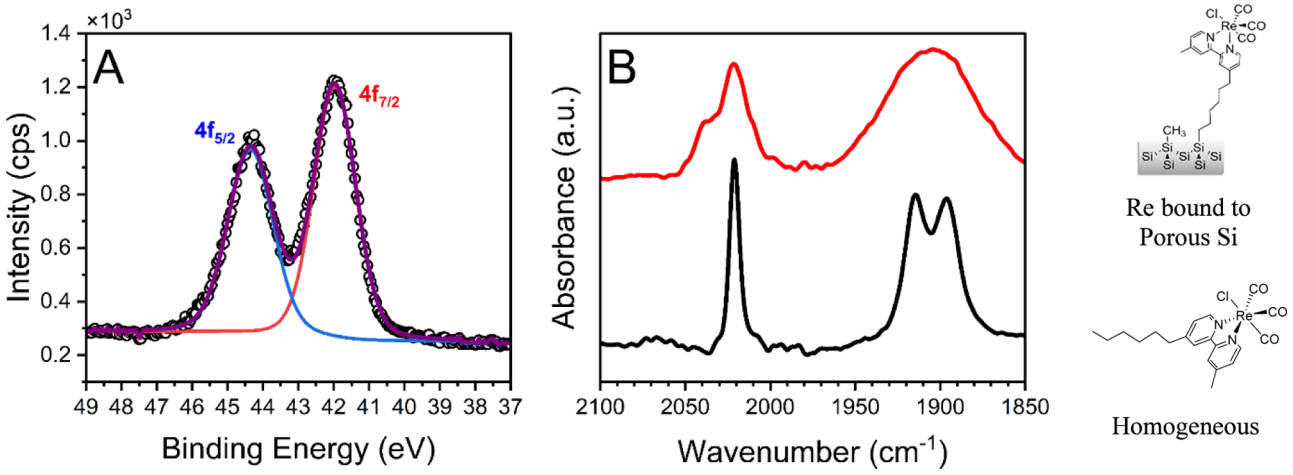

Figure 2. (A) Re 4f region of XPS of the Re complex attached to Si(111) and (B) ATR-FTIR measurements of Re attached to porous silicon (red) and the Re(4-hexyl-bpy)$(CO)_3$Cl in MeCN (black). The IR bands correspond to symmetric (2024 cm^{-1}) and asymmetric stretching modes (~1905 cm^{-1}) of the carbonyl of the complex.

RESULTS AND DISCUSSION

Synthesis and Characterization of Homogenous Re(4-Hexyl-bpy)$(CO)_3$Cl

The ligand 4-hexyl-4′-methyl-2,2′-bipyridine for the homogeneous Re(bipyridine) complex was synthesized according to literature precedent and shown in Scheme 2.[21] The ligand was characterized by ^{1}H NMR spectroscopy, showing bipyridine protons at 7.1−8.6 ppm and methyl and hexyl protons between 0.8 and 2.8 ppm (see Experimental). Re(4-hexyl-4′-methyl-bpy)$(CO)_3$Cl was synthesized according to literature procedures.[22] The homogeneous molecular Re complex was characterized by ^{1}H and ^{13}C NMR spectroscopy (Figures S3 and S4) and IR spectroscopy (Figure S5). The FTIR spectra corresponded well with other similar Re tricarbonyl compounds, with a symmetric carbonyl stretching band at 2020 cm^{-1} and asymmetric stretching bands at 1915 cm^{-1} and 1896 cm^{-1}.[22]

The CV of the homogeneous compound in acetonitrile (MeCN) with 0.1 M tetrabutylammonium hexafluorophosphate ($TBAPF_6$) under argon shows two reduction waves (Figure 1A), which are the characteristic features of the Re bipyridyl complex family. The first reduction peak at −1.88 V vs $Fc^{+/0}$ is reversible and represents a ligand-based reduction. The second reduction at −2.2 V vs $Fc^{+/0}$ is quasi-reversible and represents a metal-based reduction and dissociation of Cl-[22−24] Additionally, a third oxidation is observed at −0.55 V vs $Fc^{+/0}$, which corresponds to the oxidation of a Re−Re dimer formed under reducing conditions. Under a CO_2 atmosphere, a significant catalytic current enhancement is observed beyond the second reduction potential with I_{cat}/I_p = 55 (Figure 1B). Moreover, controlled potential electrolysis (CPE) at −2.3 V vs $Fc^{+/0}$ under CO_2 produced CO with 100% Faradaic efficiency (FE), confirming the complex's selective catalytic activity toward the CO_2 reduction reaction to CO (Figure S6).

After confirming homogeneous electrochemical CO_2 reduction at a glassy carbon electrode with Re(4-hexyl-4′-methyl-bpy)$(CO)_3$Cl, CV was performed with methyl-terminated p-Si(111) as the working electrode for a more appropriate comparison with the functionalized Si system (Figure 1C). The first and second reductions of the Re complex were at −1.32 V vs $Fc^{+/0}$ and −1.75 V vs $Fc^{+/0}$, respectively, with the dimer oxidation occurring at −0.46 V vs $Fc^{+/0}$. Catalytic current enhancement under CO_2 reduction was observed with I_{cat}/I_p = 7 (Figure 1D). Although i_{cat}/i_p is commonly used to quantify catalytic enhancement on metallic/conductive electrodes, we note that comparisons of i_{cat}/i_p here do not reflect a change in intrinsic molecular catalytic activity but instead reflect differences in electron transfer efficiency between the two electrode platforms. Whereas i_{cat}/i_p on conductive glassy carbon is limited by catalysis kinetics and diffusion, i_{cat}/i_p on p-type Si can be influenced by photogenerated carrier flux, interfacial electron transfer kinetics, and recombination of charges at the interface, resulting in reduced catalytic enhancement. CPE at −1.7 V vs $Fc^{+/0}$ under CO_2 produced 85% FE for CO without the presence of H_2 (Figure S7), confirming the selective CO_2 reduction catalytic activity of Re(4-hexyl-4′-methyl-bpy)$(CO)_3$Cl with p-type Si(111) semiconductor electrode.

Surface Attachment and Characterization

To achieve covalent attachment of the catalyst to the Si surface, we first used the hydrosilylation method with a vinyl-substituted bipyridine ligand. (Supporting Information). However, a significant challenge with this attachment strategy is the side polymerization reaction, which leads to the formation of a polymerized Re complex on the Si surface rather than a simple covalent Si−C attachment. This polymer was unstable under cathodic bias, desorbing from the surface, which may have accounted for the current loss observed in subsequent cyclic voltammetry runs. Pre- and post-CV SEM images (Figure S8) confirmed the formation of the polymer and its instability.

To avoid the polymerization issue associated with the hydrosilylation method, we employed Grignard and organolithium reactions, as shown in Scheme 1, to ensure reliable, stable covalent attachment of the catalyst. Lewis and Rose have previously used Grignard chemistry and the Li−halogen exchange reaction to modify the Si surface for photoelectrochemical experiments.[15,18−20] Utilizing these well-established methods, the Re$(bpy)(CO)_3$Cl complex with a six-carbon alkyl chain was covalently linked onto a Si surface via a Si−C bond (Scheme 1). The detailed procedure for attaching the Re complex to Si used in this study is described in the experimental section. After completion of the final Re metalation step, all samples were sonicated to remove any physiosorbed or weakly bound species before characterization. This step was found to be critical for reproducible electrochemical and spectroscopic results. Control experiments illustrating the importance of this

https://doi.org/10.1021/acs.inorgchem.6c01231
Inorg. Chem. 2026, 65, 9669−9679

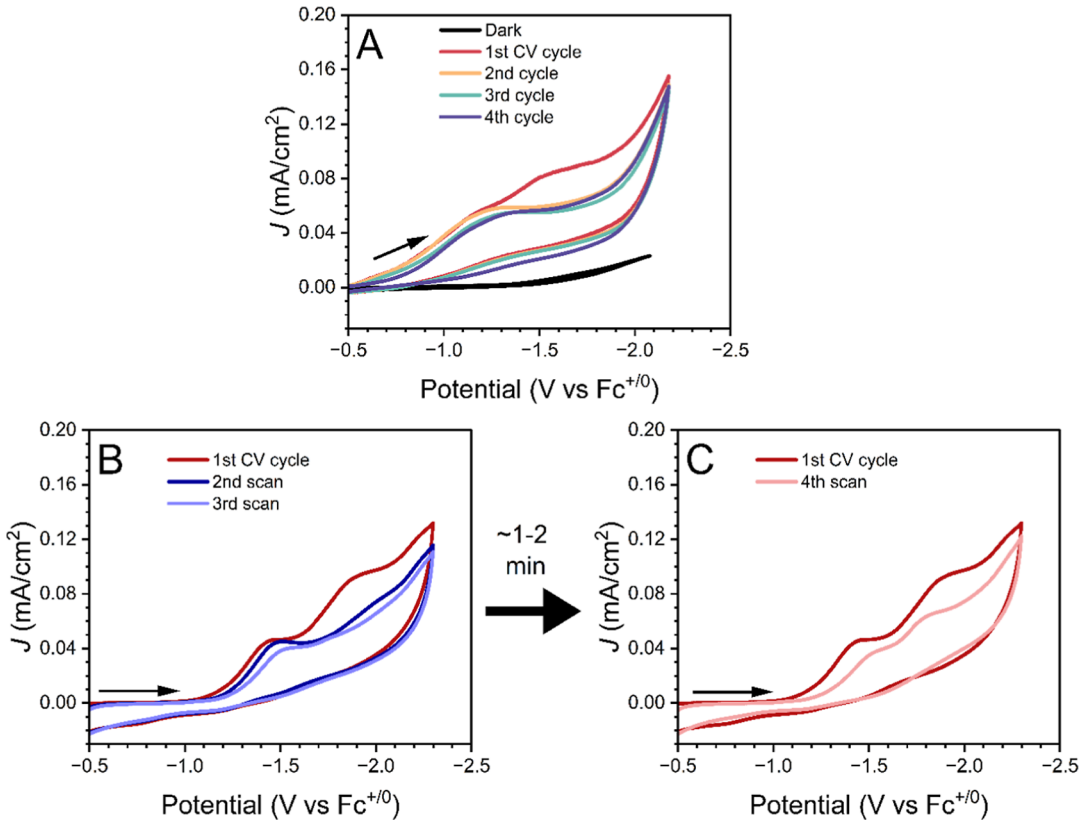

Figure 3. (A) CV of Re bipyridyl complex covalently anchored onto Si(111) surface in 0.1 M $TABPF_6$ of MeCN after 20 min of sparging the solution with Ar. (B) First to third CV cycles of Re bipyridyl complex covalently anchored onto Si(111) surface in 0.1 M TABCl of MeCN after 20 min of sparging the solution with Ar. (C) The 4th CV cycle to the first CV scan from B after 1 ∼ 2 min. Under all conditions, the cathode was illuminated with a 660 nm laser LED at 15 mW/cm^2. Scan rate was 100 mV/s. The potential was referenced to $Fc^{+/0}$ using an internal standard added after all scans were completed.

postmetalation sonication step are discussed in the following XPS and electrochemistry CV results.

ATR-FTIR Analysis of the Functionalized Surface

Re bipyridyl complex-functionalized Si was analyzed using attenuated total reflectance (ATR)-FTIR spectroscopy. To avoid confusion, we clarify that porous Si substrates were used exclusively for ATR-FTIR measurements to enhance the IR signal from surface-attached Re complexes. In contrast, all other experiments were conducted on planar Si(111) surfaces. ATR-FTIR measurements were performed at each step of the attachment described in Scheme 1 (Figure S10) to verify the completion of each reaction. The spectrum of the final sample displays the bipyridine (1470 cm^{-1} and 1620 cm^{-1}), Si-methyl (770 cm^{-1}), and the Re complex's carbonyl peaks, indicating the successful surface modification of the Si surface (Figure S10).

The IR spectrum of the Re species functionalized porous Si exhibits both symmetric and asymmetric stretching carbonyl peaks at 2024 cm^{-1} and 1905 cm^{-1}, which closely match those of the molecular Re bipyridyl complex (Figure 2B). However, compared to the molecular species, the surface-bound Re complex's IR signal shows the broadening of the carbonyl stretching frequencies, likely resulting from variations in local environments, molecular orientation, and surface interactions of the complex caused by inhomogeneous molecular packing due to the porosity of the Si surface.[25] The asymmetric band at 1905 cm^{-1} was better fit by a Gaussian model than by a Lorentzian model, confirming inhomogeneous broadening (Figure S11).

X-ray Photoelectron Spectroscopy (XPS)

The Re functionalized Si(111) surfaces were characterized by XPS. The Re 4f spectrum exhibited sharp peaks at 44.2 eV (Re $4f_{5/2}$) and 41.8 eV (Re $4f_{7/2}$) (Figure 2A), which closely match the XPS spectra of molecular Re bipyridyl derivatives,[9] as well as the Re complex attached to Si, as reported by Jia[26,27] and Huffman.[28] Additionally, the N 1s peak at 400.3 eV and the Cl 2p doublet around 199.3 eV further confirms the presence of the Re bipyridyl complex on the Si surface (Figure S13). The atomic concentration ratio of Re to N was 1:2, which aligns with the expected Re/N ratio for the Re bipyridyl complex. However, we were unable to quantify the Cl atomic concentration and calculate the Re/Cl ratio due to interference from the Si 1s plasmon peak, which obscures the Cl 2p peaks. This issue of the Cl 2p peaks being masked by the Si 1s plasmon peak has also been reported by Huffman et al.[28] As a whole, high-resolution XPS of the Re, N, and Cl regions confirms the presence of the Re bipyridyl complex on the surface of Si.

XPS was also used to demonstrate the importance of postmetalation sonication on surface cleanliness. When the sonication step was omitted, two different Re species were observed on the surface (Figure S14). While we are unable to identify the origin of the more oxidized Re species on the surface (doublet with $4f_{7/2}$ peak at 46.5 eV), it may arise from oxidation from XPS measurement, physisorbed species, or residual unreacted Re pentacarbonyl chloride reagents. However, the XPS measurement of $Re(CO)_5Cl$ reagents pressed onto carbon tape (Figure S15) exhibits peaks at 42.2 eV (Re $4f_{7/2}$) and 44.6

https://doi.org/10.1021/acs.inorgchem.6c01231
Inorg. Chem. 2026, 65, 9669−9679

eV (Re $4f_{5/2}$), indicating that the more oxidized Re signals observed on nonsonicated samples are unlikely to be from unreacted $Re(CO)_5Cl$.

The surface coverage of the Re complex was estimated using the previously reported method.[15] The area of the RSF corrected Re peak was normalized with the area of the Si 2p peak to obtain θ_{Re}, which was divided by the reported value of θ_{Me}, corresponding to the RSF corrected C−Si C 1s peak of a complete monolayer of methyl functionalized Si(111) surface, normalized with the Si 2p peak.[29] The estimated coverage was 6.0 ± 0.8%, suggesting that only a small fraction of the surface sites was functionalized with the Re bipyridyl complex.

Importantly, XPS analysis confirmed the covalent attachment of the Re bipyridyl species to the Si surface, rather than physical adsorption. The Si−C bond observed at 283.9 eV in the C 1s peak and at 100.7 eV in the Si 2p peak indicates that the Si surface is covalently linked either with the Re bipyridyl complex or the methyl group, rather than the complex being physically absorbed onto the surface (Figure S16). Aliphatic sp^2 (285.0 eV) and sp^3 (286.0 eV) carbon shifts[20] further support the presence of bipyridine, an alkyl chain, and a methyl group. Other carbon shifts at higher binding energies correspond to adventitious carbon on the surface. No significant Si oxide peak around 102 ∼ 103 eV was observed.[20,28]

Electrochemical Characterization of the Re Bipyridine Complex Functionalized Si(111)

All electrochemical measurements were performed with 0.1 M $TBAPF_6$ in MeCN, sparging with Ar for at least 20 min (for noncatalytic conditions), followed by sparging with CO_2 (for catalytic conditions). Under an inert atmosphere, CV of the Re functionalized Si(111) shows photocurrent under illumination with the characteristic two reduction features of the Re at −1.18 V vs $Fc^{+/0}$ and −1.51 V vs $Fc^{+/0}$ (Figure 3A). After the first scan, however, the second reduction feature disappears in subsequent scans, consistent with an EC process in which the second reduction (E) is followed by an irreversible chemical step corresponding to dissociation of the labile Cl ligand (C).

In the CV of the homogeneous catalyst, disappearance of the second reduction is not observed due to the replenishment of unreacted species diffusing from the bulk solution, where the concentration is higher, to the electrode. For immobilized Re species, once the Cl ligand is dissociated, it is displaced by MeCN to form solvento species $Re(R\text{-}bpy)(CO)_3(MeCN)^+$.[30,31] The two reductions of $Re(R\text{-}bpy)(CO)_3(MeCN)^+$ have a smaller peak-to-peak separation, with the second reduction occurring at milder potential compared to Cl-bound species.[31] Given this, what appears to be the one single reduction feature after the first scan for Re immobilized Si is likely the result of coalescence of the first and the second reduction features due to their proximity and the broadening of the reduction peaks.

To test the hypothesis of solvento species formation, CV was performed in 0.1 M TBACl in MeCN under the same experimental conditions (Figure 3B,C). In subsequent CV scans, the second reduction peak disappeared after the first cycle. However, after giving more than ∼1−2 min of relaxation time at open circuit potential, the second reduction peak reappeared, consistent with reversible Cl^- recoordination to the immobilized Re center and restoration of the original Cl-bound Re complex. This delayed reappearance of the second reduction peak after multiple CV cycles and an extended relaxation period indicates a slow kinetic ligand-exchange process for the immobilized species.

For samples without a sonication step, the CV in 0.1 M $TBAPF_6$ in MeCN showed behavior similar to that observed for the sonicated samples, with two reduction peaks in the first cycle, followed by the disappearance of the second peak in subsequent cycles (Figure S17). However, we observed a progressive decrease in current density across several consecutive CV scans until the signal stabilized. Because the stabilized CV response remained clearly distinct from that of bare Si−H (see Figure S8C), we infer that any loosely bound or physiosorbed species were removed during the initial CV cycles, leaving only the stable covalently bound species on the surface.

Photovoltage Calculation

Photovoltage was determined following previous literature precedent,[26,28] by comparing the reduction potentials of functionalized Re complex on p-Si(111) wafer under illumination to those of Re complex functionalized on degenerately doped n-type Si(111) in the dark (Figure 4). The estimated

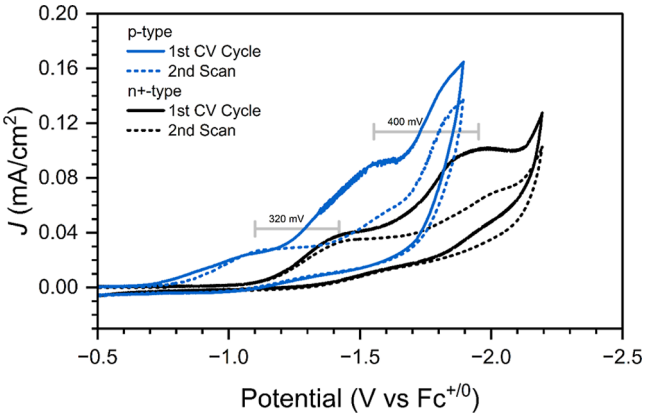

Figure 4. CV of Re bipyridyl complex covalently anchored onto Si(111) surface in 0.1 M $TABPF_6$ of MeCN after 20 min of sparging the solution with Ar. The cathode was illuminated with 660 nm laser LED with 15 mW/cm^2 power. Scan rate was 100 mV/s. Potential was referenced to $Fc^{+/0}$.

photovoltages were 320 mV and 400 mV for the first and second reductions, respectively, which fall within the reported photovoltage range of 200−600 mV for p-type Si.[32] This difference in estimated photovoltage between the first and second reductions could be explained by the irreversible nature of the second reduction, as reported by Kumar et al.[5]

Interestingly, when comparing the reduction potentials of the Refunctionalized Si electrode to those of the homogeneous Re complex on a methyl-terminated Si surface, the functionalized electrode exhibits an approximately 200 mV positive shift for both reduction events. These shifts in peak potentials may arise from multiple factors.

First, the mixed monolayer formed by the tethered Re complexes may generate additional interfacial dipoles at the Si(111) surface/electrolyte interface, thereby increasing band bending in p-type Si. Such dipole-induced tuning of band energetics by organic monolayers on the Si surface has been well established by Rose and co-workers.[18,20] Consistent with this concept, Huffman and co-workers, in their study of Re complex immobilization on Si(111) via sonochemical hydrosilylation, reported a 239 mV shift in flat-band potential between a mixed monolayer containing a surface-bound Re−phen complex

https://doi.org/10.1021/acs.inorgchem.6c01231
Inorg. Chem. 2026, 65, 9669−9679

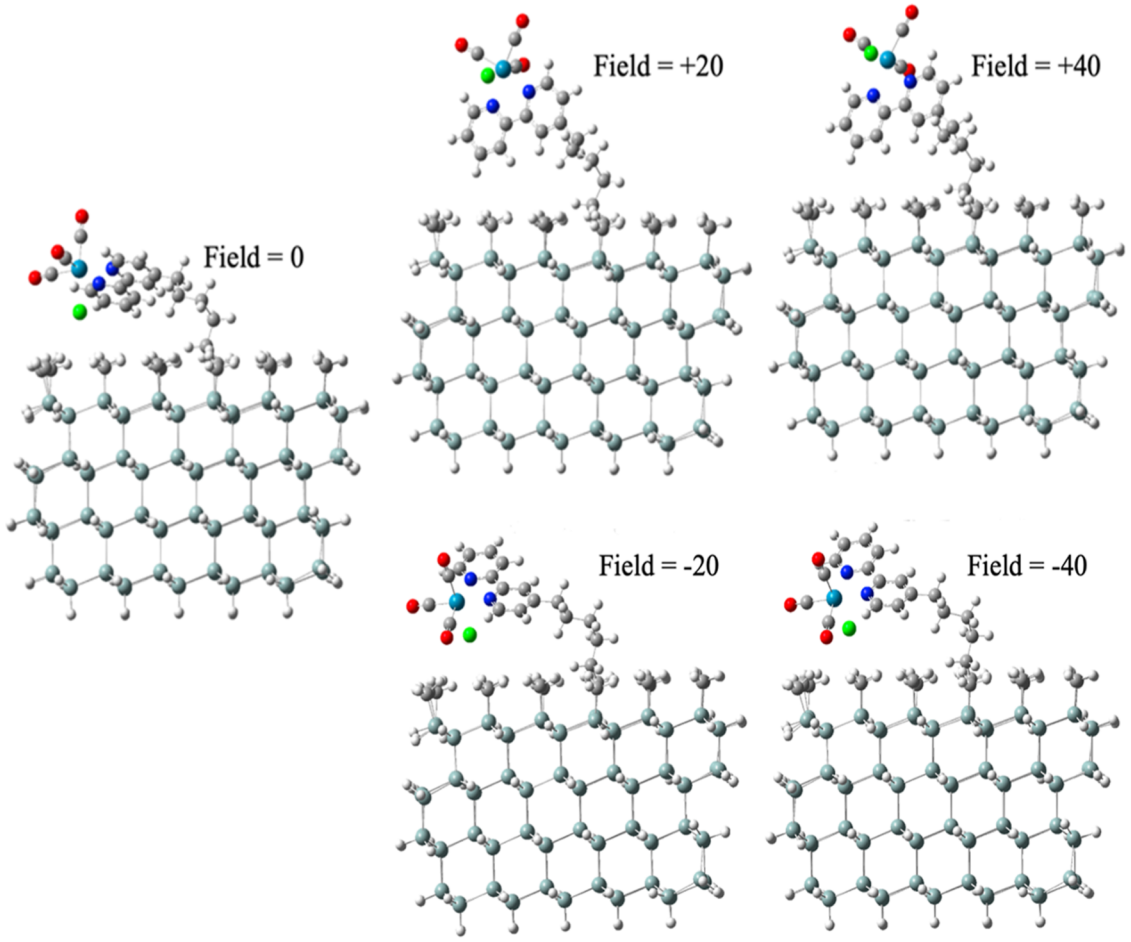

Figure 5. Comparison of geometries of Re(4-hexyl-bpy)$(CO)_3$Cl catalyst on a methylated Si(111) surface models as a 4 wide −12 long −8 deep silicon slab that has been capped with hydrogens on the sides for charge neutralization. These geometries were determined through geometry optimization under a field relative to the *Z* axis using Gaussian 16. The *Z* axis was oriented along the connecting Si−C bond between the surface and the Re catalyst. Tight optimization bounds with an ultrafine grid were used. The theory used density functional theory with a B3LYP functional and a pseudopotential basis set using 6−31g for H and C, 6−31g (d) for N,O, and Cl, and lanl2dz for Si and Re.

together with hexyl groups and a purely hexyl-terminated Si(111) surface.[28] This magnitude is comparable to the ∼200 mV positive shift observed in the Refunctionalized Si electrode relative to the homogeneous system.

Another possible explanation is that the covalent immobilization shortens the electron-transfer distance between the Si surface and the Re complex, thereby enhancing electronic coupling between the two. From the Marcus Theory perspective, this lowers the kinetic barrier for the charge transfer and the reduction of the Re complex, causing the reduction of the surface-attached Re complex to occur at a less negative applied potential. Moreover, under illumination, improved charge-transfer kinetics may suppress interfacial charge recombination (radiative or nonradiative) and enhance quasi-Fermi level splitting, thereby increasing the observed photovoltage. Similar increases in photovoltage associated with faster interfacial charge transfer in immobilized molecular systems have been reported previously.[33−35]

Rigorous evaluation of these hypotheses would require electrochemical impedance spectroscopy (EIS) and Mott−Schottky analysis to directly compare the flat-band potentials of the two systems, as well as other spectroscopic techniques, such as photoluminescence or transient absorption, to probe recombination dynamics as a function of tether length. In the present study, we limit our discussion to reporting the observed differences in peak potentials between the functionalized and homogeneous systems, while leaving detailed mechanistic investigations for our future work.

Surface Coverage Calculations

Surface coverage of the electroactive species was calculated using eq 1

$$Q = nFN \tag{1}$$

where *Q* is the total charge passed, which can be calculated by integration of the peak area in a cyclic voltammogram, *n* is the number of electrons used for reduction, *F* is the Faraday constant, and *N* represents the moles of electroactive species. Considering the reduction feature after the first scan is likely due to the coalescence of the two reduction features, the number of electrons used was 2. The moles of electroactive species, estimated with eq 1, were then divided by the density of atop site Si atoms of Si(111), 1.31×10^{-9} mol/cm^2, to yield approximately 7.4% of surface coverage of the electroactive Re complex.

It is important to note that while the XPS and the electroactive species calculations are in good agreement with each other, they may both underestimate the total Re surface coverage, while remaining important for understanding the overall system. XPS

https://doi.org/10.1021/acs.inorgchem.6c01231
Inorg. Chem. 2026, 65, 9669−9679

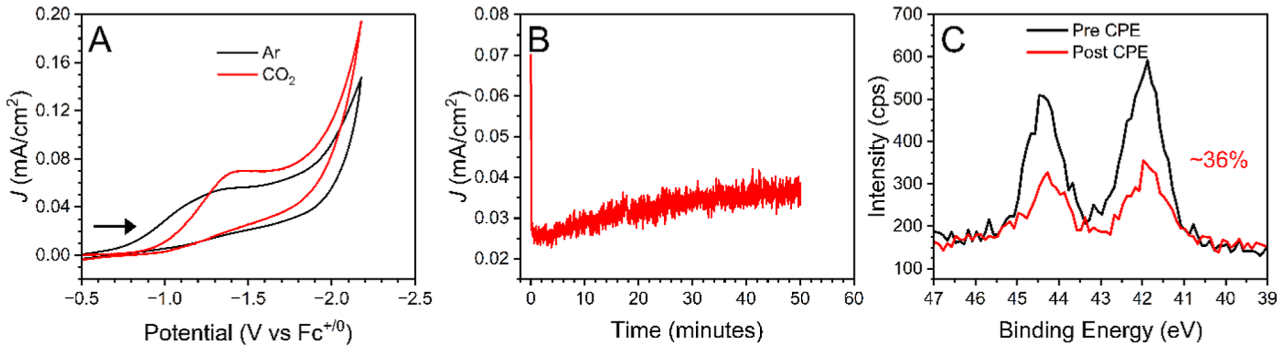

Figure 6. (A) CV of Re bipyridyl complex covalently anchored onto Si(111) surface in 0.1 M $TABPF_6$ of MeCN under CO_2 (red). The CV under CO_2 was compared to the 4th CV scan under Ar (black). Scan rate was 100 mV/s. (B) Controlled potential electrolysis (CPE) under CO_2. The cathode was illuminated with a 660 nm laser LED with 15 mW/cm^2 power. Total 4 subsequent CV runs were measured. (C). The Re 4f XPS signal of a pristine Refunctionalized Si wafer (black) and post CPE (red) showing roughly 36% of the signal is retained, indicating Re detachment from the surface under prolonged catalytic conditions.

surface analysis can vary depending on the measurement location and X-ray penetration depth. Overall, smaller differences in these can slightly alter the outcome of the experiment while still providing a good estimate of surface coverage. On the other hand, determination of the number of electroactive species via CV gives a definitive surface coverage of the catalyst involved in the electrochemical process. While this is useful for practical electrochemical understanding, such as determining a turnover rate, this method can also underestimate the amount of Re on the surface due to a range of factors, including a blocking effect that inhibits charge stabilization and, therefore, heterogeneous charge transfer, as well as resistance and capacitive charging currents.

To get a full picture of the surface, ICP−MS was performed to obtain a more accurate Re concentration on a 1 cm^2 Si(111) surface (Figure S20). The results showed an average concentration of 1.6 ppb of Re in a 50 mL HNO_3 solution obtained after dissolution of the surface-bound Re species, corresponding to 4.24×10^{-10} mol of Re. This value was divided by the surface atomic density of Si on Si(111) atop sites, 7.84×10^{-14} atoms/cm^2 (equivalent to 1.31×10^{-9} mol/cm^2), yielding an estimated surface coverage of 32.4%. Of note, this number includes coverage of Re species on both the front-polished side and back-unpolished side. Dividing the number by 2 and assuming equal functionalization on both sides would yield roughly 16% surface coverage on each side. However, since the rough, unpolished side has a higher effective surface area than the polished side, the front side is likely to have fewer Re species attached. In this case, the surface coverage on the front side would be lower than 16%, bringing it closer to the values estimated from XPS and electroactive species calculations.

The low surface coverage can be attributed to the relatively large molecular footprint of the hexane alkyl linker and the Re bipyridyl complex compared to the distance between atop-site Si atoms on the Si(111) surface. The reported kinetic diameter of hexane ranges from 4.3 Å to 10.3 Å,[36] and the diameter of the Re bipyridyl complex is roughly 9 Å, both of which exceed the 3.8 Å distance between Si atop site atoms. Consequently, 1:1 covalent attachment of the Re complex to the individual Si atop site atom is sterically hindered, unlike small methyl groups that achieve full monolayer coverage.[12] This steric effect on the surface coverage of the surface-bound molecule on the Si surface has been explored by Rose and co-workers.[37]

Computational Analysis of the Immobilized Re Species

Given the low surface coverage of 6−7%, and assuming a uniform distribution rather than island-like clustering, the immobilized Re complexes are expected to be well separated. The large spacing should allow free rotation of the alkyl linker, leading to a disordered monolayer. To explore the range of plausible configurations Re complex can take with and without applied bias, DFT geometry optimizations for the Re complex on a methylated Si surface were performed at varying strengths of applied fields (Figure 5). The applied field strengths were converted to interfacial potentials relative to the potential of zero charge (PZC) (Table S2), described in detail in the Supporting Information.

This optimization showed a preference for the complex to lie against the surface both when no field is applied and when a negative field (positive potentials relative to the PZC) is applied. The complex only moves away from the surface when positive fields (negative potentials relative to the PZC) are applied along the axis perpendicular to the surface.

It is important to note that, in these computational calculations, the Re complex was modeled as an isolated species due to the low surface functionalization and the high experimental cost and error associated with adding additional species. However, we expect that greater functionalization could introduce intermolecular interactions and steric constraints, thereby altering the accessible conformations. For example, we initially considered whether the slow EC kinetics after the second reduction could arise from unfavorable orientations in which the Cl axial ligand faces the surface, potentially restricting ligand exchange. However, the DFT optimizations do not support such a surface-blocked configuration under cathodic bias. Instead, they indicate that the Re−Cl bond is parallel to the surface at field strengths needed for catalysis. While this is more accessible than the Cl down configuration, the Cl parallel configuration still allows for possible interactions with other Re units on the surface and is less accessible than the Cl up orientation. These Re−Re unit interactions, particularly under catalytic conditions, may be responsible for slower catalytic turnover and slower surface kinetic ligand exchange. Therefore, although the present single-site model does not capture such effects, they may become relevant under conditions of increased functionalization and will be investigated further using computational models of multiple Re centers in our future work. However, this level of DFT analysis provides invaluable insight into the interactions of the Re complex at the Si surface.

https://doi.org/10.1021/acs.inorgchem.6c01231
Inorg. Chem. 2026, 65, 9669−9679

The rotation and movement of the complex indicate its ability to adopt conformations that may slow reactivity at the surface, particularly when bulky tetrabutylammonium cations, solvent, and CO_2 are taken into account, providing a reasonable explanation for the slow kinetics of the Cl^- ligand reactivity.

Catalytic Performance and Stability of the Immobilized Re Species on Si(111)

In a CO_2 environment, the current enhancement was observed relative to the final CV scan under inert conditions, indicating catalytic activity (Figure 6A). The following electrolysis at −1.9 V vs Fc+/0 for 1 h produced 15% Faradaic efficiency (FE) for CO and 54% H_2 (Figure 6B).

The catalytic current enhancement is significantly lower compared to the homogeneous catalysis of Re(4-hexyl-bpy)-$(CO)_3Cl$. For the functionalized hybrid Si, neither stirring nor reduced illumination significantly affected the catalytic current enhancement, suggesting that the current response is not limited by bulk CO_2 mass transport or light intensity (Figure S18). Therefore, the observed behavior can be attributed to a catalytically limited process, likely governed by the surface concentration and intrinsic activity of the surface-bound Re complex compared to the homogeneous system. First, and most simply, the low catalytic activity of the surface-immobilized Re complex can be attributed to its concentration (6 ∼ 7%). In addition, slow EC kinetics following the second reduction, as indicated by electrolyte-dependent CVs with TBACl, likely limit the observed current enhancements.

However, the low surface coverage and slow kinetics alone cannot explain the change in overall FE relative to the homogeneous counterpart. We therefore first considered whether surface immobilization perturbs the electronic configuration of the reduced $Re(bpy)(CO)_3$ species and affects the product selectivity. In the homogeneous Re bipyridyl complex, prior DFT studies suggest CO selectivity is attributed to the mixed metal−ligand character of the doubly reduced $[Re(R\text{-}bpy)(CO)3]^-$, with electron density in π^* orbital and another in d_z^2 orbital of Re, favoring the binding of CO_2 rather than proton.[38] In the case of surface-immobilized species, if the bpy ligand were positioned close to and lying flat on the Si surface, interactions with the methylated surface could destabilize the bpy π^* orbital and promote hybridization with the Re dz^2 orbital, favoring a more metal-centered, reduced state and, consequently, hydride formation and H_2 evolution. This hypothesis, however, is not supported by our DFT geometry optimizations, which show that Re complex moves further away from the surface at negative potentials, suggesting that the electronic-configuration perturbation is unlikely to be the reason for the FE change.

Another possibility is that the methylated Si surface contributes to H_2 production. Although Rose and Dempsey reported slower HER kinetics on the methylated Si surface compared to CO_2 reduction,[18,39] residual water in MeCN is likely the major source of H_2 generation under CO_2. CO formation is most likely due to the Re bpy catalyst, as the methylated surface alone is not expected to reduce CO_2 to CO in the absence of a molecular CO_2 reduction catalyst.

Regarding the stability of the covalently attached Re complex, XPS of the functionalized Si was measured before and after electrochemical analysis. After electrolysis, the atomic ratio of Re 4f to Si 2P is ∼36% the initial concentration (Figure 6C). The decrease in Re peak area may result from cathodic-bias-induced desorption of the immobilized complex and/or catalyst deactivation during electrolysis. Given the observed loss of Re complex, the gradual increase in current during electrolysis can therefore reflect the progressive loss/deactivation of Re sites and increased exposure or activation of HER sites, which would increase H_2 production without increasing CO formation.

CONCLUSION

Overall, the organolithium reaction and the Grignard approach for covalently attaching the Re bipyridyl complex to a Si surface yield clean anchoring of the complex. Not only is the attachment facile and prevents side reactions, but the applied voltage required for CO_2 reduction is 200 mV more positive than in the homogeneous system. This large improvement provides evidence supporting the effectiveness and potential of surface-attached catalysts on semiconducting surfaces. However, in this case, the catalytic activity of this hybrid molecular/Si photocathode was rather poor. Experimentally, we have identified that the observed poor activity and selectivity are due to slow EC kinetics of the surface-bound Re complex and catalyst deactivation and/or detachment. Importantly, our experiments indicate that the relatively low loading, low photon flux, and CO_2 diffusion to the Si surface are not responsible for the limited current enhancement.

Overall, while covalent attachment via a Si−C bond enables immobilization of the Re complex on the Si surface, our results indicate that this surface attachment alone does not reproduce, nor enhance, the activity or selectivity observed for the homogeneous molecular catalyst. Accordingly, future studies should focus on strategies that control molecular orientation and the local surface environment, including more rigid tethering motifs that enforce an active-site geometry accessible to the substrate.

EXPERIMENTAL SECTION

General Considerations

All chemical reagents were purchased from commercial sources and were used without further purification unless otherwise noted. Chlorobenzene, THF, toluene, and MeCN were sparged with nitrogen gas to remove oxygen, dried with molecular sieves before use, and stored under nitrogen. Tetrabutylammonium hexafluorophosphate ($[Bu_4N][PF_6]$, Aldrich, 98%) was recrystallized three times with ethanol and dried under vacuum for 16 h before use. XPS was performed on an SSF-Kratos AXIS-SUPRA.

Synthesis of 4-Hexyl-4′methyl-2,2′ Bipyridine. 600 mg 4,4-Dimethyl-2,2-dipyridyl was dissolved in THF in a Schlenk Flask. At −78 °C, 1.1 equiv of Lithium di-isopropylamide (LDA) was added dropwise over 1 h. After stirring for 3 h, 10 equiv of deoxygenated 1-bromopentane was added via cannula transfer, and the reaction mixture was allowed to cool to room temperature overnight. Next, the reaction was quenched by adding 10 mL of water, and the solution was washed with 10 mL of DCM three times using a separatory funnel. The collected organic layer was dried using $MgSO_4$. After solvent evaporation, the resulting oil was dissolved in Celite 545 (Thermo Scientific Chemicals), which was then purified by column chromatography on a triethylamine-washed silica column (1:0 to 7:3 hexane/ethyl acetate). Flash column chromatography was performed on a Teledyneisco CombiFlash Rf200. Yield: 264 mg (30.2%)

^1H NMR (300 MHz, $CDCl_3$): δ 8.56 (dd, J = 5.2, 3.4 Hz, 2H), 8.24 (t, J = 1.9 Hz, 2H), 7.5 (dd, J = 5.0, 1.7 Hz, 2H), 2.76−2.65 (m, 2H), 2.45 (s, 3H), 1.80−1.62 (m, 1H), 1.45−1.24 (m, 6H, bpy-$CH_2CH_2CH_2CH_2CH_2CH_3$), 0.90 (t, 3H)

Synthesis of 4-Bromohexyl-4′methyl-2,2′ Bipyridine. 600 mg 4,4-Dimethyl-2,2-dipyridyl was dissolved in THF in a Schlenk flask. At −78 °C, 1.1 equiv of Lithium diisopropylamide (LDA) was added dropwise over 1 h. After stirring for 3 h, 10 equiv of deoxygenated 1,5-

https://doi.org/10.1021/acs.inorgchem.6c01231
Inorg. Chem. 2026, 65, 9669−9679

dibromopentane was added via cannula transfer, and the reaction mixture was allowed to cool to room temperature overnight. Next, the reaction was quenched by adding 10 mL of water, and the solution was washed with 10 mL of DCM three times using a separatory funnel. The collected organic layer was dried using $MgSO_4$. After solvent evaporation, the resulting oil was dissolved in Celite 545 (Thermo Scientific Chemicals), which was then purified by column chromatography on a triethylamine-washed silica column (1:0 to 7:3 hexanes/ethyl acetate). Flash column chromatography was performed on a Teledyneisco CombiFlash Rf200. Yield: 258 mg (23.7%)

^{1}H NMR (300 MHz, $CDCl_3$): δ 8.57 (t, J = 5.4 Hz, 2H), 8.25 (t, J = 2,2 Hz, 2H), 7.19−7.11 (m, 2H), 3.42 (t, J = 6.8 Hz, 2H), 2.72 (t, J = 7.8 Hz, 2H), 2.46 (s, 3H), 1.87 (p, J = 6.9 Hz, 2H), 1.73 (p, J = 7.6 Hz, 2H), 1.46 (dp, J = 23.5, 7.5 Hz, 4H)

Synthesis of Re(4-Hexyl-4′methyl-2,2′ bipyridine)(CO)$_3$Cl. $Re(CO)_5Cl$ was dissolved in 50 mL of hot toluene in a round-bottom flask. An equimolar amount of 4-hexyl-4′metg-di-*tert*-butyl-2,2′-bipyridine was added to the hot solution, and the reaction mixture was stirred with reflux for 3 h. Once the orange color was confirmed, the solution was removed from the heat and cooled in a freezer overnight. If crystallization did not occur, the surface of the round-bottom was scratched with a glass rod to induce crystallization. The crystals that formed overnight were filtered under vacuum and dried in a vacuum oven at 90 °C.

^{1}H NMR (300 MHz, $CDCl_3$): δ 8.90 (dd, J = 5.7, 3.9 Hz, 2H), 7.99 (d, J = 9.7 Hz, 2H), 7.35 (d, J = 5.7 Hz, 2H), 2.81 (t, J = 7.8 Hz, 1H), 2.59 (s, 1H), 1.73 (p, J = 7.4 Hz, 2H), 1.47−1.31 (m, 6H), 1.73 (p, J = 7.6 Hz, 2H), 0.93 (t, 3H)

^{13}C NMR (125 MHz, $CDCl_3$): δ 197.48, 190.02, 156.08, 155.57, 155.54, 152.71, 152.60, 151.43, 128.00, 127.26, 123.97, 123.21, 35.80, 31.62, 30.24, 29.01, 22.61, 21.79, 14,17, 1.13.

Surface Functionalization. Single-sided polished boron-doped p-type (111) Si wafers were purchased from Si Valley Microelectronics (SVM), Inc. The p-type Si wafer had a resistivity range of 5−10 Ω·cm with a thickness of 500 μm. The degenerate n-tpye Si had resistivity range of 0.000 to 0.005 Ω·cm with a thickness of 475 ∼ 550 μm. Before surface modification, Si(111) samples were cleaned by sonication for 10 min each in acetone, methanol, and DI water. After rinsing with DI water and drying, all samples were washed in freshly prepared piranha solution (3:1 v/v H_2SO_4/H_2O_2) for 20 min and then rinsed with 18 MΩ water. The oxide layer was removed by immersing the samples in HF for ∼1 min, followed by immersion in deoxygenated 40% NH_4F solution for 20 min. The resulting hydrogen-terminated p-type Si samples were copiously rinsed with deoxygenated 18 MΩ water and stored in a glovebox for further surface modification.

Chlorination was performed according to the known established procedures.[15,18,20] Next, 80 mg of 4-bromohexyl-4′methyl-2,2′ bipyridine ligand was dissolved in dry THF in a Schlenk flask and reacted with 1.1 equiv of n-BuLi at −78 °C (acetone/dry ice bath). After stirring for 20 min, the solution was transferred to the flask containing freshly prepared Si−Cl samples immersed in dry THF (at −78 °C) using a cannula transfer technique. The solution containing the Si samples was cooled to room temperature for over 7 h. After rinsing with THF, the samples were placed in a 1.5 M solution of CH_3MgCl at 65 °C for 2∼4 h to fill in any unreacted Si−Cl sites with a methyl group. The final metalation step was performed by placing the ligand-attached Si samples in Re(CO)5Cl (∼10 mg) dissolved in toluene, and refluxing at 110 °C for over 1 h. The samples were thoroughly cleaned with dried toluene, followed by sonicating in acetonitrile for at least 30 min.

Electrochemistry. An Ohmic contact was made by scratching the back of the Reattached Si wafer and applying gallium−indium (Ga−In) eutectic (Sigma-Aldrich). Next, the sample was immediately transferred to a custom-made Teflon PEC cell. The O-ring diameter was 0.4 cm, exposing approximately 0.126 cm^2 of the Si wafer surface. All electrochemical measurements were performed using a BASi EC Epsilon potentiostat with a three-electrode configuration containing an $Ag/AgNO_3$ reference, a graphite counter electrode (separate by a fritted tube), and a working electrode. The electrolyte in all experiments was 0.1 M tetrabutyl ammonium hexafluorophosphate ($TBAPF_6$) in dry acetonitrile unless noted otherwise. After fully assembling the PEC cell, the solution was sparged with Ar and CO_2 for at least 20 min before electrochemical characterization. Ferrocene was added at the end of CV experiments, and its redox potential was measured with a glassy carbon electrode. A 661 nm laser diode was used as an illumination source, and an OPHIR PD300-3W-V1 photodetector and OPHIR NOVA II power monitor/meter measured the intensity of the light (∼15 mW/cm^2). Controlled potential electrolysis (CPE) was performed under the same condition used for the CV experiments, with stirring added. Gaseous products were identified and quantified using an Agilent Technologies 7890A gas chromatograph.

ATR-FTIR. Attenuated total reflectance-Fourier transform infrared (ATR-FTIR) spectra of porous Si with the Re complex immobilized were measured using a Nicolet iS50 FTIR Spectrometer equipped with a built-in wide-range diamond ATR crystal. The porous Si wafer was mounted on the ATR crystal with the functionalized surface facing the crystal. The wafer was gently pressed into contact with the crystal. The resolution was 4 cm^{-1}, and the scan number was over 256.

ICP−MS. ICP−MS was conducted on a Thermo iCAP RQ. All falcon tubes and glassware used in ICP−MS measurements were cleaned by soaking in 5 ∼ 8% HCl acid bath for at least 24 h and rinsed with 18 MΩ water before use. The Re standard concentrations of 0.1, 0.5, 0.8, 1, and 5 ppb with 5% HNO_3 solution were prepared from a Re standard purchased from Alfa Aesar (1000 μg/mL in 5% HNO_3). The Re complex-attached Si(111) samples were immersed in 70% HNO3 overnight and diluted to 5% HNO_3 before measurements.

■ ASSOCIATED CONTENT

Supporting Information

The Supporting Information is available free of charge at https://pubs.acs.org/doi/10.1021/acs.inorgchem.6c01231.

^{1}H NMR spectra for all compounds, ^{13}C NMR spectra of Re(4-hexyl-4′methyl-2,2′ bipyridine)$(CO)_3Cl$, additional experimental details for CPE, SEM images of Refunctionalized Si(111) prepared via hydrosilylation and organolithium reaction, ATR-FTIR spectra of Refunctionalized Si(111) at each step of the organolithium route, XPS spectra, CVs of Re−Si hybrid electrode without final sonication step, and CVs of Re−Si hybrid electrode under CO_2 environment without stirring and varying light intensities, ICP−MS standard curve and corresponding Re concentrations collected from 1 cm^2 Si(111) samples, applied field calculations and conversions to applied potential, and illustration of photoelectrochemical cell (PDF)

■ AUTHOR INFORMATION

Corresponding Author

Clifford P. Kubiak − *Department of Chemistry and Biochemistry, University of California San Diego, La Jolla, California 92093-0358, United States;* orcid.org/0000-0003-2186-488X; Email: ckubiak@ucsd.edu

Authors

Byunghoon Lee − *Department of Chemistry and Biochemistry, University of California San Diego, La Jolla, California 92093-0358, United States*

Christopher J. Miller − *Department of Chemistry and Biochemistry, University of California San Diego, La Jolla, California 92093-0358, United States;* orcid.org/0000-0001-8822-4823

Jessica G. Freeze − *Department of Chemistry and Energy Sciences Institute, Yale University, New Haven, Connecticut 06520, United States*

https://doi.org/10.1021/acs.inorgchem.6c01231
Inorg. Chem. 2026, 65, 9669−9679

Rajiv Ramanujam Prabhakar − *Chemical Sciences Division, Lawrence Berkeley National Laboratory, Berkeley, California 94720, United States*

Glenda Chen − *Department of Chemistry and Biochemistry, University of California San Diego, La Jolla, California 92093-0358, United States*

Saya Okuno − *Department of Chemistry and Biochemistry, University of California San Diego, La Jolla, California 92093-0358, United States*

Julianne S. Lampert − *Department of Chemistry and Energy Sciences Institute, Yale University, New Haven, Connecticut 06520, United States;* orcid.org/0009-0007-7386-8600

Victor S. Batista − *Department of Chemistry and Energy Sciences Institute, Yale University, New Haven, Connecticut 06520, United States;* orcid.org/0000-0002-3262-1237

Complete contact information is available at: https://pubs.acs.org/10.1021/acs.inorgchem.6c01231

Author Contributions

[‖]B.L. and C.J.M. contributed equally.

Notes

The authors declare no competing financial interest.

■ ACKNOWLEDGMENTS

This material is based on work performed by the Liquid Sunlight Alliance, which is supported by the U.S. Department of Energy, Office of Science, Office of Basic Energy Sciences, and Fuels from Sunlight Hub under Award no. DE-SC0021266. The authors acknowledge Dr. Ich Tran and the use of facilities and instrumentation at the UC Irvine Materials Research Institute (IMRI), which is supported in part by the National Science Foundation through the UC Irvine Materials Research Science and Engineering Center (DMR-2011967). We thank Neal Arakawa and the Environmental and Complex Analysis Laboratory (ECAL) for the ICP−MS measurement described in this literature.

■ REFERENCES

(1) Benson, E. E.; Kubiak, C. P.; Sathrum, A. J.; Smieja, J. M. Electrocatalytic and Homogeneous Approaches to Conversion of CO2 to Liquid Fuels. *Chem. Soc. Rev.* **2009**, *38* (1), 89−99.

(2) Barrett, J. A.; Miller, C. J.; Kubiak, C. P. Electrochemical Reduction of CO2 Using Group VII Metal Catalysts. *Trends Chem.* **2021**, *3* (3), 176−187.

(3) Kumar, B.; Llorente, M.; Froehlich, J.; Dang, T.; Sathrum, A.; Kubiak, C. P. Photochemical and Photoelectrochemical Reduction of CO2. *Annu. Rev. Phys. Chem.* **2012**, *63*, 541−569.

(4) Lewis, N. S. Research Opportunities to Advance Solar Energy Utilization. *Science* **2016**, *351* (6271), aad1920.

(5) Kumar, B.; Smieja, J. M.; Kubiak, C. P. Photoreduction of CO2 on P-Type Silicon Using Re(Bipy-But)(CO)3Cl: Photovoltages Exceeding 600 mV for the Selective Reduction of CO2 to CO. *J. Phys. Chem. C* **2010**, *114* (33), 14220−14223.

(6) Zhang, S.; Fan, Q.; Xia, R.; Meyer, T. J. CO2 Reduction: From Homogeneous to Heterogeneous Electrocatalysis. *Acc. Chem. Res.* **2020**, *53* (1), 255.

(7) Zhanaidarova, A.; Moore, C. E.; Gembicky, M.; Kubiak, C. P. Covalent Attachment of [Ni(Alkynyl-Cyclam)]2+ Catalysts to Glassy Carbon Electrodes. *Chem. Commun.* **2018**, *54* (33), 4116−4119.

(8) Zhanaidarova, A.; Ostrericher, A. L.; Miller, C. J.; Jones, S. C.; Kubiak, C. P. Selective Reduction of CO2 to CO by a Molecular Re(Ethynyl-Bpy)(CO)3Cl Catalyst and Attachment to Carbon Electrode Surfaces. *Organometallics* **2018**, *38*(6).

(9) Zhanaidarova, A.; Jones, S. C.; Despagnet-Ayoub, E.; Pimentel, B. R.; Kubiak, C. P. Re(tBu-Bpy)(CO)3Cl Supported on Multi-Walled Carbon Nanotubes Selectively Reduces CO2 in Water. *J. Am. Chem. Soc.* **2019**, *141* (43), 17270−17277.

(10) Rotundo, L.; Barbero, A.; Nervi, C.; Gobetto, R. CO2 Electroreduction on Carbon-Based Electrodes Functionalized with Molecular Organometallic Complexes—A Mini Review. *Catalysts* **2022**, *12* (11), 1448.

(11) Reguero, M.; Claver, C.; Carrilho, R. M. B.; Masdeu-Bultó, A. M. Immobilized Molecular Catalysts for CO2 Photoreduction. *Adv. Sustainable Syst.* **2022**, *6*, 2100493.

(12) Wong, K. T.; Lewis, N. S. What a Difference a Bond Makes: The Structural, Chemical, and Physical Properties of Methyl-Terminated Si(111) Surfaces. *Acc. Chem. Res.* **2014**, *47* (10), 3037−3044.

(13) Henriksson, A.; Neubauer, P.; Birkholz, M. Functionalization of Oxide-Free Silicon Surfaces for Biosensing Applications. *Adv. Mater. Interfaces* **2021**, *8*, 2100927.

(14) Linford, M. R.; Renter, P.; Eisenberger, P. M.; Chidsey, C. E. D. Alkyl Monolayers on Silicon Prepared from 1-Alkenes and Hydrogen-Terminated Silicon. *J. Am. Chem. Soc.* **1995**, *117* (11), 3145−3155.

(15) Lattimer, J. R. C.; Brunschwig, B. S.; Lewis, N. S.; Gray, H. B. Redox Properties of Mixed Methyl/Vinylferrocenyl Monolayers on Si(111) Surfaces. *J. Phys. Chem. C* **2013**, *117* (51), 27012−27022.

(16) Buriak, J. M. Illuminating Silicon Surface Hydrosilylation: An Unexpected Plurality of Mechanisms. *Chem. Mater.* **2014**, *26* (1), 763−772.

(17) Pekarek, R. T.; Celio, H.; Rose, M. J. Synthetic Insights into Surface Functionalization of Si(111)−R Photoelectrodes: Steric Control and Deprotection of Molecular Passivating Layers. *Langmuir* **2018**, *34* (22), 6328−6337.

(18) Gurrentz, J. M.; Rose, M. J. Non-Catalytic Benefits of Ni(II) Binding to an Si(111)-PNP Construct for Photoelectrochemical Hydrogen Evolution Reaction: Metal Ion Induced Flat Band Potential Modulation. *J. Am. Chem. Soc.* **2020**, *142* (12), 5657−5667.

(19) Bansal, A.; Li, X.; Lauermann, I.; Lewis, N. S.; Yi, S. I.; Weinberg, W. H. Alkylation of Si Surfaces Using a Two-Step Halogenation/Grignard Route. *J. Am. Chem. Soc.* **1996**, *118* (30), 7225−7226.

(20) Boucher, D. G.; Kearney, K.; Ertekin, E.; Rose, M. J. Tuning P-Si(111) Photovoltage via Molecule|Semiconductor Electronic Coupling. *J. Am. Chem. Soc.* **2021**, *143* (6), 2567−2580.

(21) Larson, S. L.; Elliott, C. M.; Kelley, D. F. Charge Separation in Donor-Chromophore-Acceptor Assemblies: Linkage and Driving Force Dependence of Photoinduced Electron Transfers. *J. Phys. Chem.* **1995**, *99* (17), 6530−6539.

(22) Smieja, J. M.; Kubiak, C. P. Re(Bipy-tBu)(CO)3Cl−improved Catalytic Activity for Reduction of Carbon Dioxide: IR-Spectroelectrochemical and Mechanistic Studies. *Inorg. Chem.* **2010**, *49* (20), 9283−9289.

(23) Sullivan, B. P.; Bolinger, C. M.; Conrad, D.; Vining, W. J.; Meyer, T. J. One- and Two-Electron Pathways in the Electrocatalytic Reduction of CO2 by Fac-Re(Bpy)(CO)3Cl (Bpy = 2,2′-Bipyridine). *J. Chem. Soc., Chem. Commun.* **1985**, 1414−1415.

(24) Johnson, F. P. A.; George, M. W.; Hartl, F.; Turner, J. J. Electrocatalytic Reduction of CO2 Using the Complexes [Re(Bpy)-(CO)3L]n (n = + 1, L = P(OEt)3, CH3CN; n = 0, L = Cl−, Otf−; Bpy = 2,2′-Bipyridine; Otf− = CF3SO3) as Catalyst Precursors: Infrared Spectroelectrochemical Investigation. *Organometallics* **1996**, *15* (15), 3374−3387.

(25) Blaudez, D.; Bonnier, M.; Desbat, B.; Rondelez, F. Two-Dimensional Polymerization in Langmuir Films: A PM-IRRAS Study of Octadecyltrimethoxysilane Monolayers. *Langmuir* **2002**, *18* (24), 9158−9163.

(26) Jia, X.; Nedzbala, H. S.; Bottum, S. R.; Cahoon, J. F.; Concepcion, J. J.; Donley, C. L.; Gang, A.; Han, Q.; Hazari, N.; Kessinger, M. C.; Lockett, M. R.; Mayer, J. M.; Mercado, B. Q.; Meyer, G. J.; Pearce, A. J.; Rooney, C. L.; Sampaio, R. N.; Shang, B.; Wang, H. Synthesis and Surface Attachment of Molecular Re(I) Complexes Supported by Functionalized Bipyridyl Ligands. *Inorg. Chem.* **2023**, *62* (5), 2359−2375.

(27) Jia, X.; Cui, K.; Alvarez-Hernandez, J. L.; Donley, C. L.; Gang, A.; Hammes-Schiffer, S.; Hazari, N.; Jeon, S.; Mayer, J. M.; Nedzbala, H. S.; Shang, B.; Stach, E. A.; Stewart-Jones, E.; Wang, H.; Williams, A. Synthesis and Surface Attachment of Molecular Re(I) Hydride Species with Silatrane Functionalized Bipyridyl Ligands. *Organometallics* **2023**, *42* (16), 2238−2250.
(28) Huffman, B. L.; Bein, G. P.; Atallah, H.; Donley, C. L.; Alameh, R. T.; Wheeler, J. P.; Durand, N.; Harvey, A. K.; Kessinger, M. C.; Chen, C. Y.; Fakhraai, Z.; Atkin, J. M.; Castellano, F. N.; Dempsey, J. L. Surface Immobilization of a Re(I) Tricarbonyl Phenanthroline Complex to Si(111) through Sonochemical Hydrosilylation. *ACS Appl. Mater. Interfaces* **2023**, *15* (1), 984−996.
(29) Nemanick, E. J.; Hurley, P. T.; Brunschwig, B. S.; Lewis, N. S. Chemical and Electrical Passivation of Silicon (111) Surfaces through Functionalization with Sterically Hindered Alkyl Groups. *J. Phys. Chem. B* **2006**, *110* (30), 14800−14808.
(30) Grice, K. A.; Gu, N. X.; Sampson, M. D.; Kubiak, C. P. Carbon Monoxide Release Catalysed by Electron Transfer: Electrochemical and Spectroscopic Investigations of [Re(Bpy-R)(CO)4](OTf) Complexes Relevant to CO2 Reduction. *Dalton Trans.* **2013**, *42*, 8498−8503.
(31) Clark, M. L.; Cheung, P. L.; Lessio, M.; Carter, E. A.; Kubiak, C. P. Kinetic and Mechanistic Effects of Bipyridine (Bpy) Substituent, Labile Ligand, and Brønsted Acid on Electrocatalytic CO2 Reduction by Re(Bpy) Complexes. *ACS Catal.* **2018**, *8* (3), 2021−2029.
(32) Laurans, M.; Wells, J. A. L.; Ott, S. Immobilising Molecular Ru Complexes on a Protective Ultrathin Oxide Layer of P-Si Electrodes towards Photoelectrochemical CO2 Reduction. *Dalton Trans.* **2021**, *50*, 10482−10492.
(33) Beiler, A. M.; McCarthy, B. D.; Johnson, B. A.; Ott, S. Enhancing Photovoltages at P-Type Semiconductors through a Redox-Active Metal-Organic Framework Surface Coating. *Nat. Commun.* **2020**, *11*, 5819.
(34) Seo, J.; Pekarek, R. T.; Rose, M. J. Photoelectrochemical Operation of a Surface-Bound, Nickel-Phosphine H2 Evolution Catalyst on p-Si(111): A Molecular Semiconductor|catalyst Construct. *Chem. Commun.* **2015**, *51*, 13264−13267.
(35) Gong, L.; Yin, H.; Nie, C.; Sun, X.; Wang, X.; Wang, M. Influence of Anchoring Groups on the Charge Transfer and Performance of P-Si/TiO2/Cobaloxime Hybrid Photocathodes for Photoelectrochemical H2 Production. *ACS Appl. Mater. Interfaces* **2019**, *11* (37), 34010−34019.
(36) Suh, B. L.; Kim, J. Reverse Shape Selectivity of Hexane Isomer in Ligand Inserted MOF-74. *RSC Adv.* **2020**, *10*, 22601−22605.
(37) Li, F.; Basile, V. M.; Pekarek, R. T.; Rose, M. J. Steric Spacing of Molecular Linkers on Passivated Si(111) PhotoelectrodesClick to Copy Article Link. *ACS Appl. Mater. Interfaces* **2014**, *6* (22), 20557−20568.
(38) Benson, E. E.; Sampson, M. D.; Grice, K. A.; Smieja, J. M.; Froehlich, J. D.; Friebel, D.; Keith, J. A.; Carter, E. A.; Nilsson, A.; Kubiak, C. P. The Electronic States of Rhenium Bipyridyl Electrocatalysts for CO2 Reduction as Revealed by X-Ray Absorption Spectroscopy and Computational Quantum Chemistry. *Angew. Chem., Int. Ed.* **2013**, *52* (18), 4841−4844.
(39) Bein, G. P.; Stewart, M. A.; Assaf, E. A.; Tereniak, S. J.; Sampaio, R. N.; Miller, A. J. M.; Dempsey, J. L. Methyl Termination of P-Type Silicon Enables Selective Photoelectrochemical CO2 Reduction by a Molecular Ruthenium Catalyst. *ACS Energy Lett.* **2024**, *9* (4), 1777−1785.

https://doi.org/10.1021/acs.inorgchem.6c01231
Inorg. Chem. 2026, 65, 9669−9679